



## RESEARCH ARTICLE

# The structural details of the interaction of single-stranded DNA binding protein hSSB2 (NABP1/OBFC2A) with UV-damaged DNA

Teegan Lawson<sup>1</sup> | Serene El-Kamand<sup>1</sup> | Didier Boucher<sup>2</sup> | Duc Cong Duong<sup>1</sup> |  
 Ruvini Kariawasam<sup>1</sup> | Alexandre M. J. J. Bonvin<sup>3</sup>  | Derek J. Richard<sup>2</sup> |  
 Roland Gamsjaeger<sup>1,4</sup>  | Liza Cubeddu<sup>1,4</sup>

<sup>1</sup>School of Science and Health, Western Sydney University, Penrith, New South Wales, Australia

<sup>2</sup>Cancer and Ageing Research Program, Institute of Health and Biomedical Innovation, Translational Research Institute, Queensland University of Technology, Woolloongabba, Queensland, Australia

<sup>3</sup>Bijvoet Center for Biomolecular Research, Faculty of Science – Chemistry, Utrecht University, Utrecht, The Netherlands

<sup>4</sup>School of Life and Environmental Sciences, University of Sydney, Sydney, New South Wales, Australia

## Correspondence

Roland Gamsjaeger and Liza Cubeddu, School of Science and Health, Western Sydney University, Penrith, NSW 2751, Australia.  
 Email: r.gamsjaeger@westernsydney.edu.au; l.cubeddu@westernsydney.edu.au

## Funding information

Western Sydney University

## Abstract

Single-stranded DNA-binding proteins (SSBs) are required for all known DNA metabolic events such as DNA replication, recombination and repair. While a wealth of structural and functional data is available on the essential human SSB, hSSB1 (NABP2/OBFC2B), the close homolog hSSB2 (NABP1/OBFC2A) remains relatively uncharacterized. Both SSBs possess a well-structured OB (oligonucleotide/oligosaccharide-binding) domain that is able to recognize single-stranded DNA (ssDNA) followed by a flexible carboxyl-tail implicated in the interaction with other proteins. Despite the high sequence similarity of the OB domain, several recent studies have revealed distinct functional differences between hSSB1 and hSSB2. In this study, we show that hSSB2 is able to recognize cyclobutane pyrimidine dimers (CPD) that form in cellular DNA as a consequence of UV damage. Using a combination of biolayer interferometry and NMR, we determine the molecular details of the binding of the OB domain of hSSB2 to CPD-containing ssDNA, confirming the role of four key aromatic residues in hSSB2 (W59, Y78, W82, and Y89) that are also conserved in hSSB1. Our structural data thus demonstrate that ssDNA recognition by the OB fold of hSSB2 is highly similar to hSSB1, indicating that one SSB may be able to replace the other in any initial ssDNA binding event. However, any subsequent recruitment of other repair proteins most likely depends on the divergent carboxyl-tail and as such is likely to be different between hSSB1 and hSSB2.

## KEYWORDS

hSSB2, DNA repair, NABP1, NMR, OBFC2A, SSB

## 1 | INTRODUCTION

Single-stranded DNA binding proteins (SSBs) are essential in humans as they protect temporarily exposed single-stranded DNA that exists as a consequence of all known DNA metabolic events including DNA replication, recombination, and repair.<sup>1</sup> SSB proteins typically

recognize single-stranded DNA (ssDNA) via a highly conserved oligonucleotide-binding (OB) domain that is made up of a five-stranded bent antiparallel  $\beta$ -sheet that form a closed  $\beta$ -barrel. SSBs also possess additional structured or unstructured regions that are important in protein-protein interactions modulating downstream processing of DNA. In addition to the main SSB that exists in humans, RPA, we

have over the last decade characterized two more important SSBs, hSSB1 (NABP2/OBFC2B/SOSSB1) and hSSB2 (NABP1/OBFC2A/SOSSB2),<sup>1-16</sup> both of which possess a single ssDNA binding OB domain.

Although only very few differences exist between the sequences of the OB domains of the two SSBs, several studies have revealed distinct roles of hSSB2 in contrast to hSSB1. For example, in the thymus of mice, mSSB2 but not mSSB1 has been implicated in the regulation of the ROR (retinoid-related orphan receptor) gene, a gene that plays a significant role in many physiological processes.<sup>17</sup> Similarly, higher expression levels of mSSB2 compared to mSSB1 have been observed in the testis, spleen, and thymus, potentially indicating a specific role of mSSB2 in repair and recombination in these tissues.<sup>18</sup> Another study also revealed significant functional differences between mSSB1 and mSSB2 involvement in skeletogenesis.<sup>19</sup> One possible explanation for these observed differences is the significantly different sequence of the flexible carboxyl-tail that is not involved in the interaction with ssDNA but is able to recruit other proteins, possibly by being distinctively post-translationally modified.<sup>16</sup> However, the existence of small but potentially significant molecular differences in the binding of the SSBs to ssDNA cannot be excluded as no detailed structural data on the OB domain of hSSB2 are available to date.

In this work, we show that hSSB2 is able to recognize cyclobutane pyrimidine dimers (CPD) that form in the DNA as a consequence of UV damage. Using our published NMR data on the OB domain of hSSB2 and a combination of biolayer interferometry (BLI) and NMR titration experiments, we have calculated a structural model revealing hSSB2 OB binding to CPD-containing ssDNA. These data provide for the first time the molecular details of how hSSB2 recognizes damaged DNA and also demonstrate the structural similarities between hSSB1 and hSSB2.

## 2 | MATERIAL AND METHODS

### 2.1 | Cell culture and cell transfection

HeLa cells were cultured in RPMI (Gibco, ThermoFisher Scientific) complemented with 10% FBS (Gibco, ThermoFisher Scientific), kept in a humidified atmosphere at 37 °C and 5% CO<sub>2</sub>. HeLa cells were transfected with control stealth siRNA vs stealth siRNA against (full-length) hSSB2 (Invitrogen, Life Technologies, HSS148948). Individual siRNA sequences were 5'-GAAUAGUAAUUGGGUACAGGUACA-3' (sense) and 5'-UGUACCUGUACCCAUUUACUUAUUC-3' (antisense). siRNAs were transfected using RNAiMax (Life Technologies) in OptiMEM (Gibco, ThermoFisher Scientific).

### 2.2 | Clonogenic assay

Forty-eight hours after transfection with control and hSSB2 siRNAs, 200 cells were plated in six well plates. Cells were irradiated 6 hours after plating with an UVC source (UVC transilluminator). Dosimetry was carried out in house. After 12 days incubation, cells were washed with PBS before staining with crystal violet (0.01%) and 20% ethanol

solution for 10 minutes at room temperature. After washing wells with water, colonies (>50 cells) were counted and reported to untreated samples with UVC to determine the cell surviving fraction in percent.

### 2.3 | Immunofluorescence

Transfected cells with control and hSSB2 siRNA were radiated with 5 J/m<sup>2</sup> UVC and immediately after exposure fixed with PFA 4% in PBS for 20 minutes at room temperature. After two washes of PBS, fixed cells were incubated 10 minutes on ice with 0.2% Triton X-100 in PBS (Triton buffer) and blocked in PBS with 3% BSA for 1 hour. For CPD staining, an extra step for DNA denaturation was added with 1 M HCl for 5 minutes and then washed three times with PBS. Cells were incubated with the primary (Thymidine dimer antibody, Sigma) and secondary antibody (mouse Alexa 488, Invitrogen) for 1 hour each at room temperature, followed by a 5 minutes incubation with DAPI, and washed with PBS. The coverslips were mounted on a slide with Prolong Gold (ibidi). Images were acquired with a DeltaVision system (GE Healthcare) and analyzed with Fuji software (>50 cells per experiment).

### 2.4 | Protein expression and purification

An *Escherichia coli* codon-optimized construct of hSSB2 OB (1-125) and corresponding mutants (GeneArt) were directionally cloned into a pGEX6p vector (with an N-terminal GST expression tag) using *Bam*HI and *Eco*RI restriction sites. Protein expression of this construct was achieved in BL21(DE3) *E. coli* cells and induced with 0.2 mM IPTG at 20 °C for 16 hours in a biofermentor for <sup>15</sup>N labeled proteins (using <sup>15</sup>N NH<sub>4</sub>Cl as nitrogen source) and in flasks for unlabelled proteins. The harvested cells were lysed via sonication in lysis buffer for NMR (10 mM MES, pH 6.0, 50 mM NaCl, 3 mM TCEP, 0.5 mM PMSF, 0.1% Triton X-100) or BLI (10 mM Phosphate, pH 6.9, 50 mM NaCl, 3 mM DTT, 0.5 mM PMSF, 0.1% Triton X-100). The soluble fraction extracted using centrifugation was purified via GSH affinity chromatography, followed by HRV-3C protease cleavage at two times 1-hour intervals and then overnight at 4°C (leaving five additional residues GPLGS, on the N-terminus of the OB construct). The cleaved protein was loaded onto a HiTrap HP Heparin (GE) column equilibrated with either NMR buffer (10 mM MES, pH 6.0, 50 mM NaCl, 3 mM TCEP) or BLI buffer (10 mM Phosphate, pH 6.9, 50 mM NaCl, 3 mM DTT). A 500-mL linear gradient consisting of 50-1000 mM NaCl in NMR or BLI buffer was used to elute hSSB2<sub>1-125</sub> protein and mutants. After exchange into either NMR or BLI buffer and a subsequent concentrating step (using 3 K cut-off), SDS-PAGE was utilized to confirm protein purity. The concentration of all proteins was determined using the theoretical extinction coefficient and the absorbance value at 280 nm.

### 2.5 | Biolayer interferometry

The BLI steady-state analysis was performed using a set of 7-8 hSSB2<sub>1-125</sub> concentrations ranging from 0.78 μM to 50 μM. Proteins

were bound to a 5' biotinylated ssDNA oligonucleotide (5'-AAATT [CPD]TT-3') in triplicate (CPD represents the cyclobutane pyrimidine dimer; HPLC purified; purchased from TriLink Biotechnologies), using the BLItz biosensor system (ForteBio). Streptavidin biosensors (ForteBio) were equilibrated in a buffer containing 10 mM HEPES and 100 mM NaCl (pH 7) for 24 hours prior to use. For each individual binding curve, an initial baseline was carried out (30 seconds), followed by the binding of the oligonucleotide to the biosensor until saturation (60 seconds). Two further baselines (30 seconds each) were carried out to transition from the initial buffer to the BLI buffer. Each construct (in BLI buffer) was allowed 120 seconds to reach an equilibrium state, followed by a 60 seconds dissociation step in BLI buffer. Average BLI equilibrium values were taken from the sensorgrams, plotted against the respective protein concentrations and fitted using the Hill Equation (1:1 stoichiometry, steady-state model) in Origin 9.1 (Microcal).

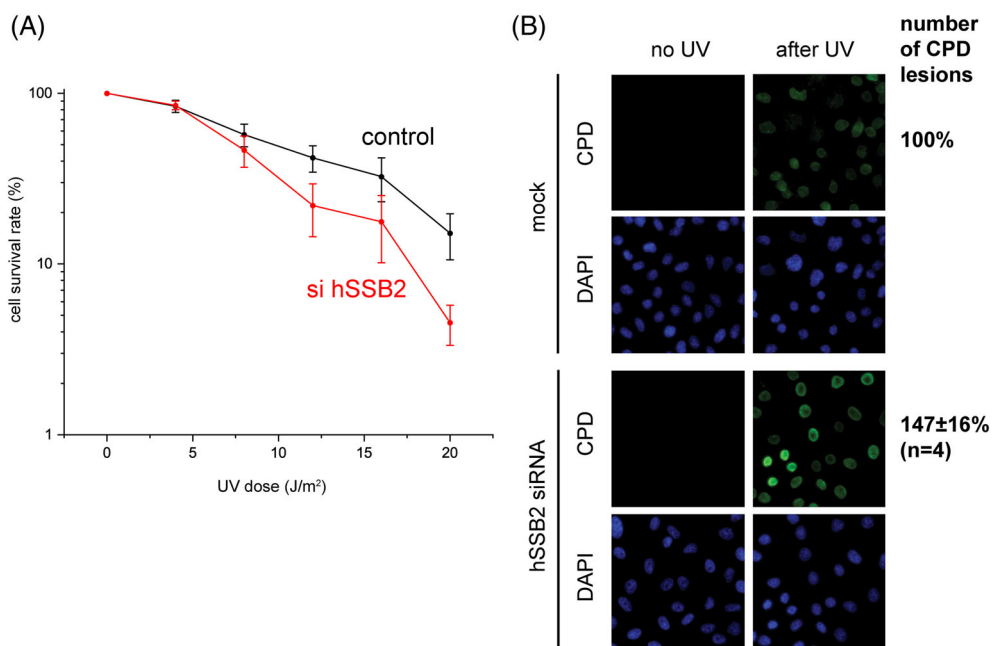
## 2.6 | NMR spectroscopy and data processing

NMR experiments were performed using approximately 0.1–0.5 mM hSSB2<sub>1–125</sub> in NMR buffer containing 10% D<sub>2</sub>O. Proton chemical shifts were referenced to 4,4-dimethyl-4-silapentanesulfonic acid (DSS) at 0 ppm. NMR spectra were recorded on either an 800 MHz or 600 MHz spectrometer (Bruker Avance III) equipped with 5-mm TCI cryoprobes at 298 K and all proton and nitrogen resonances were taken from our previously published study<sup>20</sup> (BMRB database accession number 27184). The chemical shifts of ssDNA-bound <sup>15</sup>N hSSB2<sub>1–125</sub> were unambiguously identified by gradual additions of 0.2, 0.4, 0.6, 0.8, and 1 equimolar volumes of an ssDNA oligo with the sequence 5'-TT(CPD)TT-3' (HPLC purified; purchased from TriLink Biotechnologies). The data collected were processed using Topspin (Bruker Biospin) and assignments were analyzed using Sparky (Goddard and Kneller, University of California at San Francisco).

## 2.7 | Structure calculation and HADDOCK modeling

A model of the protein structure of hSSB2 (residue 6–113 containing the OB domain) was calculated using the program CS-ROSETTA<sup>21,22</sup> using the published protein resonances from the BMRB database (BMRB database accession number 27184). The best 10 structural models, together with an ssDNA oligo containing a CPD constructed in silico using the structure of the ssDNA within the complex structure of hSSB1-6T as a template<sup>14</sup> were used as input for HADDOCK<sup>23,24</sup> (using a local installation of HADDOCK2.2). Based on our BLI and NMR data, the same ambiguous interaction restraints (AIRs) used for the calculation of the hSSB1-6T structure (base-stacking between the four key aromatics W59, Y78, W82, and Y89 and the corresponding ssDNA bases) were utilized as inputs in three separate runs, where the position of the CPD was varied relative to the aromatic residues (run 1: CPD between Y78 and W59, run 2: CPD between W59 and Y89 and run 3: CPD between Y89 and W82). No models could be obtained in runs 1 and 2, however, 250 structural models calculated in run 3 were analyzed based on their structural similarity to the hSSB1-6T complex.<sup>14</sup> The best 10 structural models were subject to a further semi-flexible refinement in HADDOCK, using AIRs incorporating both the key aromatic as well as residues that exhibit significant chemical shifts in the NMR experiments. For both calculations, hSSB2 protein residues 18–20, 33–43, 56–63, 75–96 were defined as semi-flexible based on our BLI and NMR data and all bases of the ssDNA were defined as semi-flexible and flexible. Additional restraints to maintain base planarity between the four aromatic residues (W59, Y78, W82, and Y89) and the ssDNA bases were used in the calculations in accordance with our earlier study on hSSB1.<sup>14</sup> The 10 conformers with the lowest HADDOCK score (out of a total of 250 poses) were analyzed and visualized using PyMol (Schrödinger, NY). The structural coordinates of the lowest-energy hSSB1-ssDNA-CPD model were deposited into the Figshare

**FIGURE 1** hSSB2 is required in the response to UV-triggered DNA damage. A. Clonogenic assays revealing that the absence of hSSB2 (red curve) leads to decreased survival rates of cells treated with increasing doses of UV C radiation. B. Representative images of HeLa cells probed for CPD (green) immediately after UV C irradiation; DAPI staining is shown in blue. Note that hSSB2 depletion significantly affects cyclobutane pyrimidine dimers (CPD) clearance in cells exposed to UV radiation [Color figure can be viewed at [wileyonlinelibrary.com](http://wileyonlinelibrary.com)]



data repository (DOI: 10.6084/m9.figshare.8156621) as the RCSB PDB database does not currently accept molecular models.

### 3 | RESULTS

#### 3.1 | hSSB2 is important for cell survival and CPD clearance in cells exposed to DNA damage by UV radiation

While hSSB2 has been shown to be involved in the repair of double-strand breaks (DSBs),<sup>25</sup> its role in the response to DNA damage triggered by UV radiation is not known. To address this, we initially carried out clonogenic assays in HeLa cells where we knocked down hSSB2 using siRNA and tested cell survival rates after UV radiation (Figure 1A). Notably, distinctively more cells die in the absence of hSSB2 at increasing doses of UV radiation, strongly indicating that hSSB2 plays an important role in the repair of UV-damaged DNA.

UV radiation is associated with the formations of cyclobutane pyrimidine dimers (CPD) resulting in a distortion of the double-stranded DNA molecule, opening up the two ssDNA strands and creating a “bubble” in the oligonucleotide sequence at the site of the CPD.<sup>26</sup> Thus, to determine the role of hSSB2 in the processing of these DNA damage products, we examined the CPD damage distribution and clearance in hSSB2-depleted cells (Figure 1B). As seen in the figure, the number of CPDs not removed by repair is significantly higher ( $147\% \pm 16\%$ ) when hSSB2 is knocked down compared to the control (100%) immediately after UV exposure. These data reveal that hSSB2 is involved very early in this DNA repair process and might be required for clearance of these lesions that form as a consequence of UV radiation. Given the ability of hSSB2 to recognize ssDNA,<sup>10</sup> it is very likely that the protein is also capable of directly binding to the CPDs, potentially initializing the repair process.

To determine in more detail the involvement of hSSB2 in these DNA repair processes, we have carried out a more comprehensive functional study (Boucher et al, 2019, manuscript submitted for

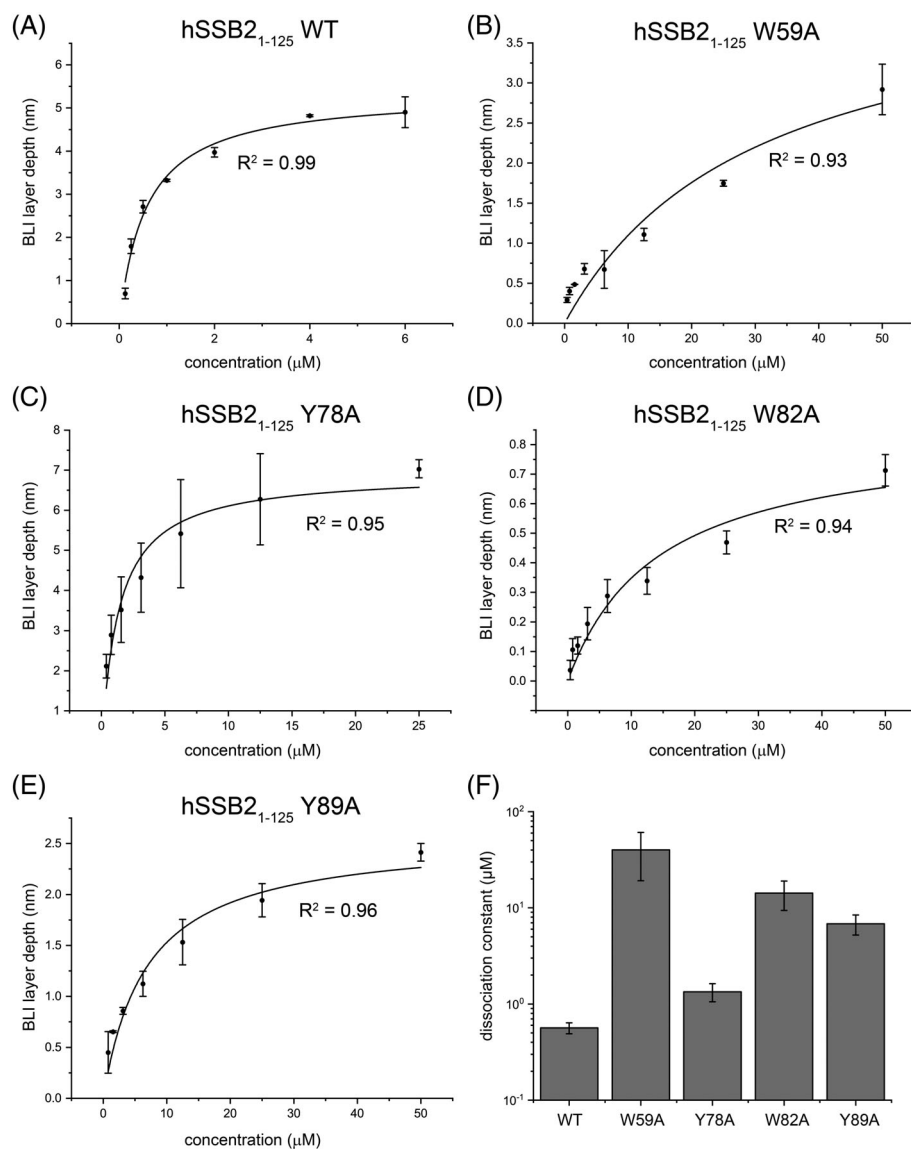


**FIGURE 2** The four key aromatic residues (W59, Y78, W82, and Y89) that are conserved in hSSB1 are critical for hSSB2 binding to CPD-containing ssDNA. A-E, Average steady-state equilibrium BLI values from  $n = 3-4$  independent TT(CPD) TT oligo binding experiments of wild-type hSSB2<sub>1-125</sub> and mutants (as indicated) are shown and fitted to a 1:1 binding model (Hill equation). F, Summary of dissociation constants of all mutants and wild-type hSSB2<sub>1-125</sub> binding to CPD-containing ssDNA

publication). We confirmed that hSSB2 is involved very early in the repair of UV-induced DNA damage by promoting the recruitment of RPA and that the protein is capable of recognizing very short stretches of ssDNA that are formed within a DNA duplex at CPD-damaged sites. However, the exact underlying molecular mechanism of CPD recognition remains unclear and is the subject of the present study.

### 3.2 | The key ssDNA binding aromatics are conserved between hSSB1 and hSSB2

We have already established earlier that hSSB2 is capable of binding to short oligonucleotide sequences<sup>20,27</sup>; to first analyze in detail binding to CPD, we carried out BLI experiments using a 6T ssDNA oligo containing a CPD in the center [TT(CPD)TT] and a hSSB2 construct

encompassing the entire OB domain (hSSB2<sub>1-125</sub>) (Figure 2A). The BLI data was fitted to a 1:1 binding model as the ssDNA binding footprint of the closely related human SSB, hSSB1, is 5 to 6<sup>14</sup> and revealed a dissociation constant of approximately 0.6  $\mu\text{M}$  which is slightly smaller than the one determined for hSSB1 (Figure 2F). We have also recently determined the structural basis of ssDNA binding to hSSB1.<sup>14</sup> Using NMR and BLI approaches we have identified four key aromatic residues (W55, Y74, F78, and Y85) in hSSB1 that are essential for the recognition of ssDNA. To test whether the conserved aromatic residues in hSSB2 (W59, Y78, W82, and Y89; refer to Figure 1 in our earlier study<sup>14</sup>) might play a similar role in the binding of CPD-containing ssDNA, we made a series of point mutants within the hSSB2<sub>1-125</sub> construct where we replaced each aromatic residue by alanine and carried out BLI experiments to test for ssDNA binding (Figure 2B-E)

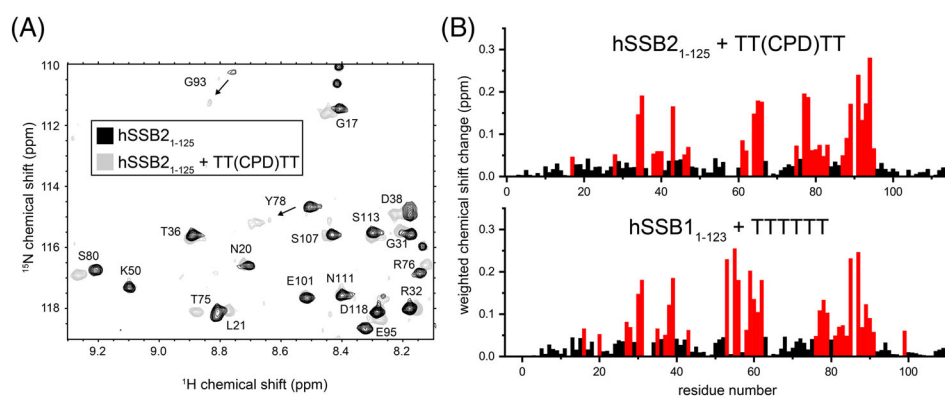


**FIGURE 3** NMR analysis of hSSB2<sub>1-125</sub> OB domain in complex with CPD-containing ssDNA revealing close similarities to hSSB1. Sections of <sup>15</sup>N-HSQC spectrum of hSSB2<sub>1-125</sub> construct in the absence (black) and presence (1:1 mixture, light gray) of TT(CPD)TT oligo, respectively. Assignments and directions of movement are indicated. B, Weighted backbone chemical shift changes of HN and N atoms for hSSB2<sub>1-125</sub> upon binding to CPD-containing ssDNA. Residues exhibiting changes larger than the average are colored in red. The ssDNA (oligo-6T) binding profile of hSSB1<sub>1-123</sub> (taken from Ref. <sup>14</sup>) is shown as a comparison [Color figure can be viewed at [wileyonlinelibrary.com](http://wileyonlinelibrary.com)]

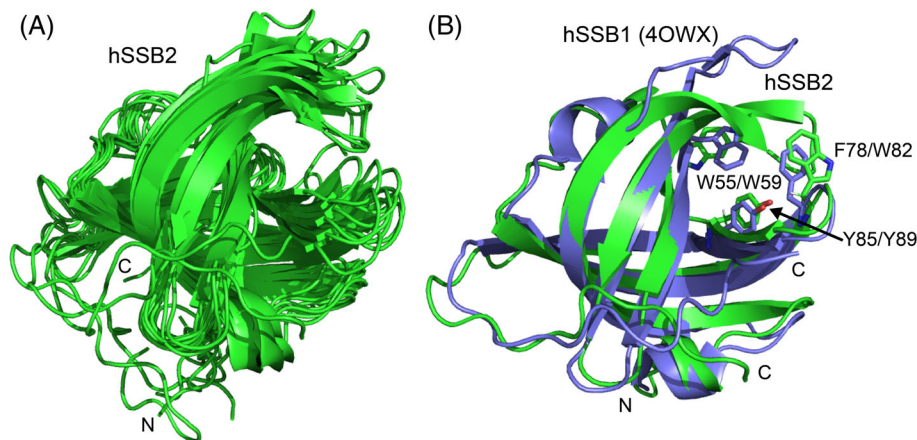


**FIGURE 4** The structural model of the OB domain of hSSB2 is highly similar to hSSB1. A, The 10 hSSB2 OB-fold structural models with the best HADDOCK score (residues 6-113) as calculated by CS-ROSETTA using the available chemical shift resonances<sup>20</sup> (BMRB database accession number 27184) as input are shown. Note that the average RMSD over all atoms of the OB domain is 3.0 Å. B, Structural overlay of the hSSB2 OB-fold model with the fourth-best HADDOCK score onto hSSB1<sup>31</sup> (taken from the PDB database ID 4OWX) demonstrating the high structural similarity displayed between hSSB2 and hSSB1 (RMSD 1.1 Å). Note that the position of the aromatic residues (stick representation) is conserved. The orientation of the hSSB2 structure is the same as in A [Color figure can be viewed at [wileyonlinelibrary.com](http://wileyonlinelibrary.com)]

using the CPD-containing ssDNA oligo. Comparison of the dissociation constants of all hSSB2<sub>1-125</sub> constructs revealed that all mutant hSSB2<sub>1-125</sub> proteins exhibit significantly weaker binding compared to the wild-type protein (Figure 2F). These data strongly indicate that all four aromatic residues are involved in the same base-stacking mechanism that is central to the hSSB1-ssDNA interaction.<sup>14</sup>

### 3.3 | Structural properties of hSSB2 ssDNA binding are identical to hSSB1

Next, to determine the molecular details of CPD-ssDNA binding, we recorded HSQC NMR experiments of hSSB2<sub>1-125</sub> in the absence and

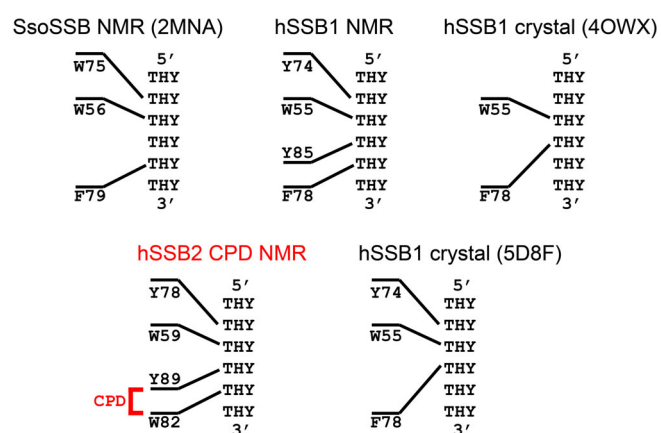


**FIGURE 5** Schematic showing the relative position of all aromatic residues that are involved in base-stacking in relation to their corresponding ssDNA bases in all known hSSB1, hSSB2 and *Sulfolobus solfataricus* SSB (SsoSSB) crystal and NMR structures and structural models. The structural data was taken from the PDB database (PDB IDs 2MNA, 4OWX, and 5D8F) and the Figshare data repository (doi: 10.6084/m9.figshare.3422788). Note that due to the relative distances to the ssDNA bases, W82 and Y89 are the only aromatic residues that are capable of base-stacking with the CPD (shown in red) [Color figure can be viewed at wileyonlinelibrary.com]

presence of the TT(CPD)TT oligo, respectively (Figure 3A). Calculation of weighted chemical shift changes<sup>28</sup> for hSSB2 upon binding to the ssDNA using the backbone assignments determined earlier<sup>20</sup> revealed a set of key binding residues (colored in red in Figure 3B). Notably, the chemical shift profile of hSSB2<sub>1-125</sub> binding to TT(CPD)TT is highly similar to that of hSSB1<sub>1-123</sub> binding to 6T (Figure 3B)<sup>14</sup> further confirming that the structural details of ssDNA recognition are conserved between hSSB1 and hSSB2.

### 3.4 | hSSB2 structural models based on chemical shift data are similar to hSSB1

In an attempt to determine the NMR-based structure of CPD-containing ssDNA-bound hSSB2 we initially recorded 3D <sup>13</sup>C and <sup>15</sup>N-NOESYs and filtered NOESY experiments at different temperatures. However, in analogy to hSSB1,<sup>14</sup> the insufficient quality of these spectra due to intermediate exchange phenomena prevented us from obtaining any intermolecular NOEs in order to calculate any structures. To circumvent these issues, CS-ROSETTA<sup>21,22</sup> in combination with our deposited chemical shifts (BMRB database accession number 27184)<sup>20</sup> were utilized to determine a structural model of the OB domain of hSSB2 (Figure 4). The best 10 model structures from the CS ROSETTA calculations are shown in Figure 4A and overlay with an RMSD of 3.0 Å over the OB domain (residues 6-113). Comparison of the crystal structure of hSSB1 (PDB 4OWX) with the most similar hSSB2 structural model reveals an RMSD of 1.1 Å (Figure 4B), demonstrating the high degree of structural similarity between the OB domains of hSSB1 and hSSB2. In addition, the positions of the key aromatic residues (W59, Y78, W82, and Y89 in hSSB2 vs W55, Y74, F78, and Y85 in hSSB1) are well conserved (Figure 4B). Taken together with the data from the mutational analysis (Figure 2) and the NMR experiments (Figure 3), this strongly indicates that the base-stacking mechanism of these four aromatic residues that drives the hSSB1-ssDNA interaction is preserved in hSSB2.

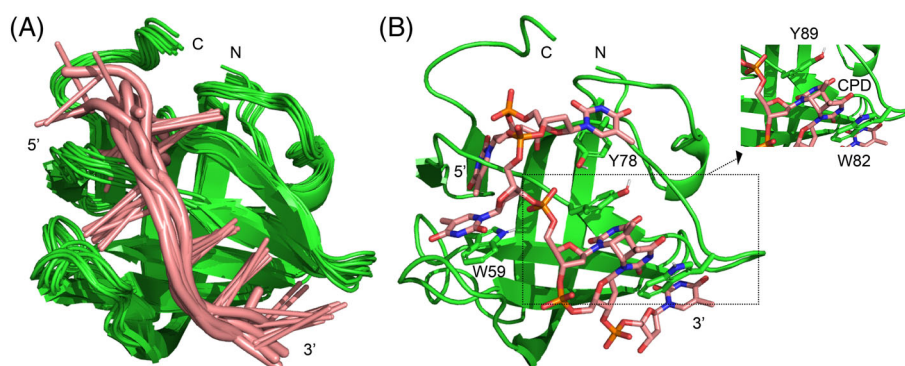


**FIGURE 6** The hSSB2-OB-CPD-ssDNA complex solution model. A, Overlay of family of 10 hSSB2-OB-CPD-ssDNA HADDOCK complex structural models with the lowest total HADDOCK score in cartoon representation. B, Cartoon (hSSB2) and stick (CPD-ssDNA) representation of the complex structural model with the lowest HADDOCK score (deposited into the Figshare data repository DOI: 10.6084/m9.figshare.8156621). The four aromatic residues (W59, Y78, W82, and Y89) that intercalate with the ssDNA and the CPD are indicated. The orientation of the hSSB2 model is the same as in A

### 3.5 | A structural model of CPD-ssDNA recognition by hSSB2

In order to gain more insight into the structural details of CPD recognition by hSSB2 we next calculated a model of the hSSB2-CPD-ssDNA complex using the program HADDOCK version 2.2<sup>23,24</sup> and our CS-ROSETTA-based hSSB2 OB-fold structural model (Figure 4). To achieve this, based on the high structural similarities between hSSB1 and hSSB2, we utilized a similar set of restraints that was used for hSSB1<sup>14</sup> taking into account the conserved base-stacking mechanism between the four key aromatics (W59, Y78, W82, and Y89) and the corresponding ssDNA bases. In these calculations, the relative position of the CPD with respect to the aromatic residues was varied within the ssDNA sequence, however, models could only be obtained with the oligo where the CPD is located between the aromatic residues W82 and Y89 (Figure 5). This is perhaps not surprising given the position of all the other hSSB2 key aromatic residues relative to the corresponding ssDNA bases which are conserved in all determined hSSB1 and *Sulfolobus solfataricus* (SsoSSB) SSBs structures (Figure 5). As can be seen in the figure, W82 and Y89 are the only aromatic residues that stack with the ssDNA in such a way that enables the two corresponding thymines to form a connected dimer (CPD).

The 10 structural models with the best HADDOCK scores are shown in Figure 6A (RMSD 0.5 Å). The two thymines are part of the CPD base-stack with W82 and Y89, respectively, as mentioned above (Figure 6B). While all thymines that form II/II-stacking are well-structured, the remaining thymine bases are disordered and do not exhibit any interactions with the ssDNA. These data confirm that—in analogy to hSSB1—four thymines including the ones that form the CPD are required to recognize the ssDNA [minimal binding sequence: TT(CPD)]. The HADDOCK calculations also revealed three hSSB2 OB-fold residues (T34, T87, and R92) that were involved in hydrogen bonds with different ssDNA bases in at least five of the 10 best structural models. Interestingly, two of these three (T34 and R92) have also been shown to be important for ssDNA recognition in the hSSB1-ssDNA complex (corresponding to hSSB1 residues T30 and R88).

## 4 | DISCUSSION AND CONCLUSIONS

Our structural model provides insight into how the OB domain of the previously relatively uncharacterised protein hSSB2, a close homolog of the better known hSSB1, binds cyclobutane pyrimidine dimers (CPDs) that form as a result of UV radiation. Given the ability of hSSB2 to also recognize unmodified ssDNA with a similar affinity<sup>27,29</sup> it is highly likely that protein molecules are bound to both the CPD and the exposed ssDNA (opposite the CPD) within the distorted double-stranded DNA in the initial stages of DNA repair.

The hSSB2-CPD complex structural model reveals essentially the same binding mechanism that hSSB1 utilizes to bind ssDNA, indicating that hSSB1 may also be able to recognize CPDs. However, recognition of the CPD takes place very early in the DNA repair process and is followed by the recruitment of a set of other important proteins.<sup>30</sup> As the interaction of both hSSB1 and hSSB2 with other proteins is also

modulated by the flexible carboxyl-terminus that does not display any similarity between the two SSBs, it is likely that hSSB1 is not able to fully replace hSSB2 in this DNA repair process. Indeed, our latest functional study (Boucher et al, 2019, manuscript submitted for publication) revealed important differences between hSSB1 and hSSB2 in the context of UV-triggered DNA repair.

In light of our structural data revealing the high degree of similarity between ssDNA binding of hSSB1 and hSSB2 it is now also clear that any functional differences observed between the SSBs, particularly in mice (mouse analogues mSSB1 and mSSB2)<sup>17–19</sup> must be due to their divergent carboxy-tails.

In our recent work on hSSB1 binding to ssDNA, we have commented on the differences seen between the published crystal structure of the OB domain of hSSB1 bound to ssDNA<sup>31</sup> and our NMR-based solution model.<sup>14</sup> Interestingly, in contrast to the published crystal structure (PDB ID 4OWX), a recently deposited crystal structure (PDB ID 5D8F) reveals base-stacking of Y74 (Y78 in hSSB2) in good agreement with both our hSSB1 and hSSB2 structural model, respectively (Figure 5). However, neither crystal structure shows an involvement of Y85 (Y89 in hSSB2) in ssDNA binding, which differs from our NMR-derived structural models. Despite these differences, the positions of the stacking aromatic residues relative to the ssDNA bases are conserved in all known NMR-based structures (Figure 5). As a consequence, the only possible location of the CPD within the ssDNA in the hSSB2-CPD-ssDNA model is between the two aromatics W82 and Y89 (Figure 5).

In summary, we have revealed the molecular details of hSSB2 binding to CPD-containing ssDNA that forms as a result of UV radiation in cells. Our structural data confirm the role that four key aromatic residues (W59, Y78, W82, and Y89) play in the binding and also demonstrate a high degree of structural similarity between ssDNA recognition of hSSB1 and hSSB2.

## ACKNOWLEDGMENTS

We would like to thank Dr Ann Kwan from the University of Sydney for expert advice and maintenance of NMR spectrometers.

## ORCID

Alexandre M. J. J. Bonvin  <https://orcid.org/0000-0001-7369-1322>

Roland Gamsjaeger  <https://orcid.org/0000-0003-1095-2569>

## REFERENCES

1. Richard DJ, Khanna KK. Single-stranded DNA binding proteins involved in genome maintenance. In: Khanna K., Shiloh Y. (eds.), *The DNA Damage Response: Implications on Cancer Formation and Treatment*. Dordrecht: Springer. 2009;349–366.
2. Ashton NW, Bolderson E, Cubeddu L, O'Byrne KJ, Richard DJ. Human single-stranded DNA binding proteins are essential for maintaining genomic stability. *BMC Mol Biol*. 2013;14:9.
3. Ashton NW, Loo D, Paquet N, O'Byrne KJ, Richard DJ. Novel insight into the composition of human single-stranded DNA-binding protein 1 (hSSB1)-containing protein complexes. *BMC Mol Biol*. 2016;17(1):24.

4. Ashton NW, Paquet N, Shirran SL, et al. hSSB1 phosphorylation is dynamically regulated by DNA-PK and PPP-family protein phosphatases. *DNA Repair (Amst)*. 2017;54:30-39.
5. Bolderson E, Petermann E, Croft L, et al. Human single-stranded DNA binding protein 1 (hSSB1/NABP2) is required for the stability and repair of stalled replication forks. *Nucleic Acids Res*. 2014;42(10):6326-6336.
6. Croft LV, Ashton NW, Paquet N, Bolderson E, O'Byrne KJ, Richard DJ. hSSB1 associates with and promotes stability of the BLM helicase. *BMC Mol Biol*. 2017;18(1):13.
7. Kariawasam R, Touma C, Cubeddu L, Gamsjaeger R. Backbone (1)H, (13)C and (15)N resonance assignments of the OB domain of the single stranded DNA-binding protein hSSB1 (NABP2/OBFC2B) and chemical shift mapping of the DNA-binding interface. *Biomol NMR Assign*. 2016;10(2):297-300.
8. Paquet N, Adams MN, Ashton NW, et al. hSSB1 (NABP2/OBFC2B) is regulated by oxidative stress. *Sci Rep*. 2016;6:27446.
9. Paquet N, Adams MN, Leong V, et al. HSSB1 (NABP2/OBFC2B) is required for the repair of 8-oxo-guanine by the hOGG1-mediated base excision repair pathway. *Nucleic Acids Res*. 2015;43(18):8817-8829.
10. Richard DJ, Bolderson E, Cubeddu L, et al. Single-stranded DNA-binding protein hSSB1 is critical for genomic stability. *Nature*. 2008;453(7195):677-681.
11. Richard DJ, Cubeddu L, Urquhart AJ, et al. hSSB1 interacts directly with the MRN complex stimulating its recruitment to DNA double-strand breaks and its endo-nuclease activity. *Nucleic Acids Res*. 2011;39(9):3643-3651.
12. Richard DJ, Savage K, Bolderson E, et al. hSSB1 rapidly binds at the sites of DNA double-strand breaks and is required for the efficient recruitment of the MRN complex. *Nucleic Acids Res*. 2011;39(5):1692-1702.
13. Touma C, Adams MN, Ashton NW, et al. A data-driven structural model of hSSB1 (NABP2/OBFC2B) self-oligomerization. *Nucleic Acids Res*. 2017;45:8609-8620.
14. Touma C, Kariawasam R, Gimenez AX, et al. A structural analysis of DNA binding by hSSB1 (NABP2/OBFC2B) in solution. *Nucleic Acids Res*. 2016;44(16):7963-7973.
15. Croft LV, Bolderson E, Adams MN, et al. Human single-stranded DNA binding protein 1 (hSSB1, OBFC2B), a critical component of the DNA damage response. *Semin Cell Dev Biol*. 2019;86:121-128.
16. Lawson T, El-Kamand S, Kariawasam R, Richard DJ, Cubeddu L, Gamsjaeger R. A structural perspective on the regulation of human single-stranded DNA binding protein 1 (hSSB1, OBFC2B) function in DNA repair. *Comput Struct Biotechnol J*. 2019;17:441-446.
17. Kang HS, Beak JY, Kim YS, et al. NABP1, a novel ROR $\gamma$ -regulated gene encoding a single-stranded nucleic-acid-binding protein. *Biochem J*. 2006;397(1):89-99.
18. Boucher D, Vu T, Bain AL, et al. Ssb2/Nabp1 is dispensable for thymic maturation, male fertility, and DNA repair in mice. *FASEB J*. 2015;29(8):3326-3334.
19. Feldhahn N, Ferretti E, Robbiani DF, et al. The hSSB1 orthologue Obfc2b is essential for skeletogenesis but dispensable for the DNA damage response in vivo. *EMBO J*. 2012;31(20):4045-4056.
20. Kariawasam R, Knight M, Gamsjaeger R, Cubeddu L. Backbone (1)H, (13)C and (15)N resonance assignments of the OB domain of the single stranded DNA-binding protein hSSB2 (NABP1/OBFC2A) and chemical shift mapping of the DNA-binding interface. *Biomol NMR Assign*. 2018;12(1):107-111.
21. Shen Y, Lange O, Delaglio F, et al. Consistent blind protein structure generation from NMR chemical shift data. *Proc Natl Acad Sci USA*. 2008;105(12):4685-4690.
22. Shen Y, Vernon R, Baker D, Bax A. De novo protein structure generation from incomplete chemical shift assignments. *J Biomol NMR*. 2009;43(2):63-78.
23. Dominguez C, Boelens R, Bonvin AM. HADDOCK: a protein-protein docking approach based on biochemical or biophysical information. *J Am Chem Soc*. 2003;125(7):1731-1737.
24. van Zundert GCP, Rodrigues J, Trellet M, et al. The HADDOCK2.2 web server: user-friendly integrative Modeling of biomolecular complexes. *J Mol Biol*. 2016;428(4):720-725.
25. Li YJ, Bolderson E, Kumar R, et al. hSSB1 and hSSB2 form similar multiprotein complexes that participate in DNA damage response. *J Biol Chem*. 2009;284(35):23525-23531.
26. Kemmink J, Boelens R, Koning TM, Kaptein R, van der Marel GA, van Boom JH. Conformational changes in the oligonucleotide duplex d(GCGTTGCG) x d(CGCAACGC) induced by formation of a cis-syn thymine dimer. A two-dimensional NMR study. *Eur J Biochem*. 1987;162(1):37-43.
27. Gamsjaeger R, Kariawasam R, Bang LH, et al. Semiquantitative and quantitative analysis of protein-DNA interactions using steady-state measurements in surface plasmon resonance competition experiments. *Anal Biochem*. 2013;440(2):178-185.
28. Ayed A, Mulder FA, Yi GS, Lu Y, Kay LE, Arrowsmith CH. Latent and active p53 are identical in conformation. *Nat Struct Biol*. 2001;8(9):756-760.
29. Flores JK, Kariawasam R, Gimenez AX, et al. Biophysical characterisation and quantification of nucleic acid-protein interactions: EMSA, MST and SPR. *Curr Protein Pept Sci*. 2015;16(8):727-734.
30. Spivak G. Nucleotide excision repair in humans. *DNA Repair (Amst)*. 2015;36:13-18.
31. Ren W, Chen H, Sun Q, et al. Structural basis of SOSS1 complex assembly and recognition of ssDNA. *Cell Rep*. 2014;6(6):982-991.

**How to cite this article:** Lawson T, El-Kamand S, Boucher D, et al. The structural details of the interaction of single-stranded DNA binding protein hSSB2 (NABP1/OBFC2A) with UV-damaged DNA. *Proteins*. 2020;88:319–326. <https://doi.org/10.1002/prot.25806>